Hydrodynamic instability leading to *Monami*

by

Ravi Shanker Singh

B.Sc., Banaras Hindu University; Varansi, India, 2006

M.Sc.(Physics), Indian Institute of Technology-Bombay; Mumbai, India, 2008

A dissertation submitted in partial fulfillment of the
requirements for the degree of Doctor of Philosophy
in Department of Physics at Brown University

PROVIDENCE, RHODE ISLAND

May 2014

This dissertation by Ravi Shanker Singh is accepted in its present form

by Department of Physics as satisfying the

dissertation requirement for the degree of Doctor of Philosophy.

Date_____   _____

Shreyas Mandre, Ph.D., Advisor

Recommended to the Graduate Council

Date_____   _____

J. Tang, Ph.D., Reader

Date_____   _____

Tom Powers, Ph.D., Reader

Approved by the Graduate Council

Date_____   _____

Sheila Bonde, Dean of the Graduate School

Vitae

Acknowledgements

Abstract of " Hydrodynamic instability leading to *Monami* " by Ravi Shanker Singh, Ph.D., Brown University, May 2014

Contents

List of Tables

List of Figures

CHAPTER ONE

Introduction

1.0.1 Motivation

Seagrasses are submerged flowering plants found in shallow marine waters, mostly in the littoral zones of freshwater and in large expanses of low lying coastal shore, they occupy less than 0.05% of the ocean areas but contribute directly to about 15% of the total biomass production in the ocean. Seagrasses plays crucial role in protecting sea shores. The extensive root system in seagrasses, which extends both vertically and horizontally, helps stabilize the sea bottom in a manner similar to the way land grasses prevent soil erosion. With no seagrasses to diminish the force of the currents along the bottom, numerous beaches, businesses, and homes can be subject to greater damage from storms.

Seagrasses provide food, shelter, and essential nursery areas to commercial and recreational fishery species and to countless invertebrates living in seagrass communities. Some fish, such as seahorses and lizardfish, can be found in seagrasses throughout the year, while other fish remain in seagrass beds during certain life stages. While some organisms, including the endangered Florida manatee and green sea turtle, graze directly on seagrass leaves, others use seagrasses indirectly to provide nutrients. Bottlenose dolphins are often found feeding on organisms that live in seagrass areas. Detritus from bacterial decomposition of dead seagrass plants provides food for worms, sea cucumbers, crabs, and filter feeders such as anemones and ascidians. Further decomposition releases nutrients (such as nitrogen and phosphorus), which, when dissolved in water, are re-absorbed by seagrasses and phytoplankton.

The relative safety of seagrass meadows provides an ideal environment for the female fishes to to lay and hatch their eggs. The safety of seagrass meadows are also useful for the juvenile fish and invertebrates to conceal themselves from predators. Seagrass leaves are also ideal for the attachment of larvae and eggs, including those

of the sea squirt and mollusk. Much of Florida's recreationally and commercially important marine life can be found in seagrass meadows during at least one early life stage. While seagrasses are ideal for juvenile and small adult fish for escape from larger predators, many infaunal organisms (animals living in soft sea bottom sediments) also live within seagrass meadows. Species such as clams, worms, crabs, and echinoderms, like starfishes, sea cucumbers, and sea urchins, use the buffering capabilities of seagrasses to provide a refuge from strong currents. The dense network of roots established by seagrasses also helps deter predators from digging through the substratum to find infaunal prey organisms. Seagrass leaves provide a place of anchor for seaweeds and for filter-feeding animals like bryozoans, sponges, and forams.

Seagrasses help trap fine sediments and particles that are suspended in the water column, which increases water clarity. When a sea floor area lacks seagrass communities, the sediments are more frequently stirred by wind and waves, decreasing water clarity, affecting marine animal behavior, and generally decreasing the recreational quality of coastal areas. Seagrasses are also known to sequester CO_2, mix and recycle the nutrients necessary for life of its inhabitants they also work to filter nutrients that come from land-based industrial discharge and stormwater runoff before these nutrients are washed out to sea and to other sensitive habitats such as coral reefs.

The primary requirement for active marine eco-systems are presence of sunlight and a mechanism to mix and transport the nutrients. Since sunlight can penetrate only near the surface of water, the sea-shores are ideal place for rich marine ecology. One of the other important factor in proliferating the marine ecology near the ocean shores is the presence of regular wave and tides which constantly stir the region, a mechanism which is not present in the lakes. Despite shallow average depth of lakes (e.g. average depth of Lake Erie is 18.6m and that of lake Chand is 4 m) with

plenty of sunlight, lakes are not able to support a rich ecology as compared to the coastal shore due to absence of tidal mixing. The coastal oceans are about 10 times as productive as the lakes. Along with marshes and mangroves, seagrasses meadows rank highest in terms of biomass production.

The ability of seagrass meadows to engineer the habitat for effective ecosystems is directly related to its ability to influence hydrodynamic processes. This requires balance between two competing requirements such as flow should be sufficiently slow so that species don't get flushed along with the water, but not stagnant and thus allowing the nutrients and other material to be transported by the flow. It is widely believed that many systems including seagrass rely on flow for the transportation and mixing of nutrients, pollens, sperms etc. A simple estimate of mixing-strength in absence of any flow instability can be estimated to help us understand the importance of existence of flow instability. A typical seagrass patch extend from $10^2 m$ to $10^3 m$ with a typical flow speed of $0.1 m/s$ to $1 m/s$, indicating that any tracer particle carried by the flow would take about $\tau = 10^2 - 10^4 s$ to cross the patch. In the absence of any flow instability mean flow is horizontal and vertical transportation and mixing of material can happen only through turbulent diffusivity $\kappa = 0.1 Ud$, where $U \approx 1 cm/s$ is the mean flow in canopy, and $d \approx 1 cm$ is characteristic length scale of plant such as its diameter or leave with. This estimate indicates that transportation of material above the grass bed can only penetrate about $\sqrt{\kappa\tau} = 3 - 30 mm$, compared to the canopy height of 10-100 cm. However in presence of flow instability even a modest 10% conversion of horizontal flow to vertical velocity results in penetration length scale of about 10-1000 cm. Indeed, It is widely believed that the phenomenon of large amplitude coherent oscillation of marine grass, known as *Monami* is a result of flow instability, much like coherent waves commonly observed on terrestrial grass field, known as *Honami* in strong wind. While the two cases seems superficially similar, there are major difference such as atmospheric flow is essentially unbounded.

Another major difference the two is the considerable difference of stiffness of canopies.

1.0.2   Previous Work

While considerable research is done to understand the phenomenon associated with atmospheric flows through terrestrial canopies, research for the case of flow through aquatic vegetation is not prevalent. Evidence of the effect of aquatic plants on unidirectional flow emerges from various study of research groups interested in conveyance of water through vegetated canals (Kouwen 1992), the cycling of particulate and dissolved matter etc. One such systematic study on the topic of blue mussels larvae settlement attributed the excess presence of blue-muscel larvae on the tip of grass to the presence of *Monami* (Grizzle 1996). The most notable research work related to *Monami* are laboratories study of open channel flow through flexible and rigid canopies [9**?**], which shows existence of coherent eddies propagating on canopy top.

The current explanation of *Monami* is proposed by Ghisalberti and Nepf [8, 9] which is inspired by the work of Raupach for the case of terrestrial canopies, which is based on Kelvin-Helmholtz (KH) instability. According to this mechanism the essential role of vegetation is to exert drag on the flow slowing it down, and giving rise to velocity differential between the canopy and the region above it. This so called shear layer profile is then expected to be hydrodynamically unstable to KH instability and break down into coherent vortices. The flexibility of grass blades then merely aids in visualizing there vortices by deforming as they are advected past by the flow. According to this shear layer model, the velocity profile of flow through vegetation can be approximated to a characteristic shear like profile - " one where
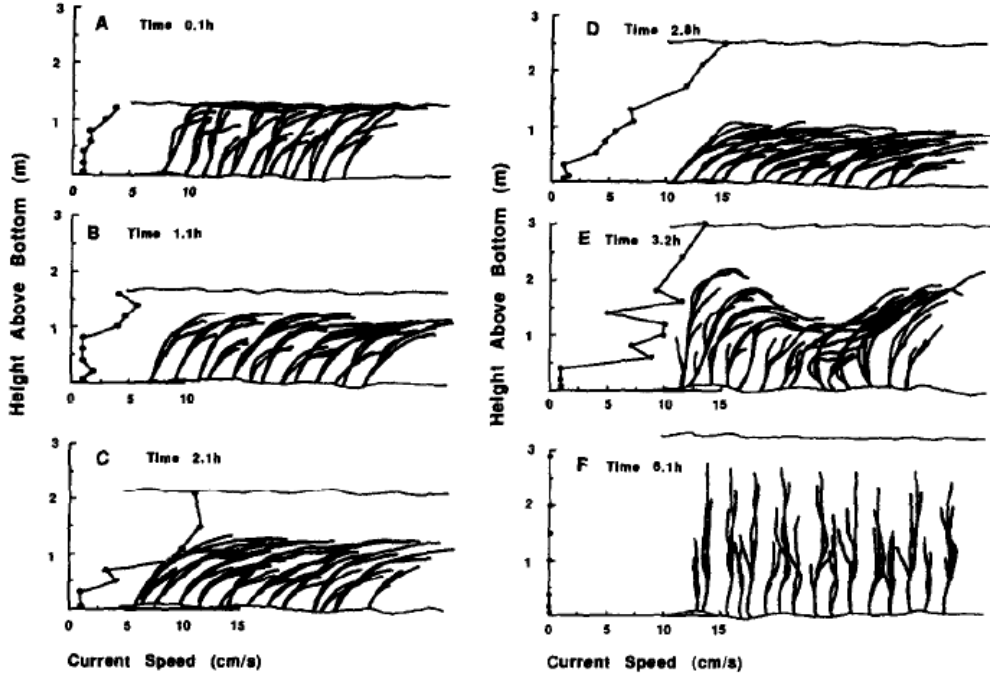
Figure 1.1: Sketches made by Grizzle, et al. [6] from direct observations of eelgrass blades in the mouth of the Jordan river, ME, USA, in response to a tidal flow through half a tidal cycle. The horizontal velocity profile is also plotted with each of the sketches. The grass spontaneously starts to wave in frame E, when the flow speed exceeds a threshold of 10-15 cm/s.

shear does not arise from the boundary condition" e.g. $U(y) = \Delta U[1 + \tanh(y/\delta)]$, in an approximately unbounded domain $-\infty < y < \infty$, using the shear layer thickness δ determined by fitting to the measured mean velocity profile (e.g. see 3.1), the frequency predicted by KH instability agrees well with the laboratories observations.

However, several aspects of existing theory remain unexplained. First, the assumption of instability of perturbation to shear layer through a mechanism of Kelvin-Helmholtz relies on absence of any interaction between the flow perturbation and drag, making shear layer a inconsistent theory. Second, classical free shear flow is known to be unstable for all the Reynolds number. On the contrary, a threshold flow speed is observed in the field for the grass to spontaneously wave [6]; below this threshold speed the grass bends steadily in response to steady current. This threshold speed corresponds to a critical Reynolds number $\approx O(1000)$, based on turbulent

viscosity. These drawbacks of existing theory suggest that flow through vegetation requires further investigation for better understanding of phenomenon.

1.0.3 Our Approach

In this study, we developed a mathematical model for the linear stability incorporating presence of grass through a drag field in the momentum equation of fluid. Although monami is manifested in the motion of grass, the drag exerted by the vegetation on the flow is central to the hypothesized instability. A linear stability analysis of this model shows that a competition between destabilizing effect of shear and stabilizing effect of drag dissipation leads to a critical flow condition characterized by Reynolds number above which flow becomes unstable leading to *Monami*. Our linear stability analysis predicts existence of two different modes of instability which we termed as mode-1 and mode-2. Mode-1 is found to be instability localized on the length scale of shear layer formed near the canopy top whereas Mode-2 is represent the flow instability on the scale of full water column. We found that mode-1 shares many of characteristics of Kelvin-Helmholtz instability such as instability on the scale of shear layer thickness but is found to have significant differences as well. The prediction of critical Reynolds number and waving frequency associated with *Monami* is found to compare well the experimental observations. Results from our analysis can also be applicable to many other related scenario such as flow over coral reefs, permeable sediments, flow through urban environments and therefore is expected to have wider impact.

Chapter Two

Mathematical Model

Given the range of length scales in the canopy (leaf thickness < 1mm, leaf width ∼ 1cm, canopy height ∼ $1m$, vegetation patch $10^2 - 10^3 m$), a fully resolved direct numerical solution is challenging and unnecessary. We instead exploit this separation of length scale between the canopy scale and its microstructure, and resort to modeling the aquatic vegetation as a homogenized multiphase medium which occupies no volume but exert drag on the fluid flow. Because the leaves are wide but thin , the volume fraction of vegetation is less than 10% in the densest of seagrass canopies, and dominant interaction with the surrounding water is by exerting a drag. Hence to leading order, we ignore the space occupied by the grass in the fluid mass and momentum balance. Further, lab scale experiments have shown that flow instability and resulting flow structure leading to monami are present even when the flexible grass is replaced with rigid dowels [8, 5]. Therefore to develop essential mathematical model we assume grass to be rigid and oriented vertically (along y direction) on average. Since the flow structure leading to monami is dominantly 2 dimension, we assume a two dimensional model for simplicity of calculation. In our mathematical model vegetation is assumed to be sufficiently dense so that drag exerted by the grass can be modeled as a continuum field.

Here we present methods for averaging the flow equations in presence of vegetation. Following Pedras & de Lemos we first average over a time interval τ which is longer than the vegetation scale velocity fluctuation time, then perform spatial averaging. Denoting overbar to represent time averaged properties and the angel brackets to denote spatial averaged properties, for any fluid property ϕ such as velocity, pressure etc.

$$\overline{\phi}(x, y, z, t) = \frac{1}{\tau} \int_{t}^{t+\tau} \phi \, dt \qquad \langle \overline{\phi} \rangle = \frac{1}{A} \int_{A} \overline{\phi} \, dx \, dy$$

$$\phi = \overline{\phi} + \phi^{'} \qquad \overline{\phi} = \langle \overline{\phi} \rangle + \phi^{''}$$

Upon performing temporal averaging of Navier-Stokes and fluid continuity equation we arrive the following equations for fluid continuity and momentum balance.

$$\frac{\partial \overline{u_i}}{\partial x_i} = 0$$

$$\rho \left[\frac{\partial \overline{u_i}}{\partial t} + \overline{u_j} \frac{\partial \overline{u_i}}{\partial x_j} \right] = -\frac{\partial \overline{p}}{\partial x_i} + \mu \frac{\partial^2 \overline{u_i}}{\partial x_j^2} - \rho \frac{\partial \overline{u_i' u_j'}}{\partial x_j}$$

(2.1)

and further spatial averaging gives

$$\frac{\partial \langle \overline{u_i} \rangle}{\partial x_i} = 0$$

$$\rho \left[\frac{\partial \langle \overline{u_i} \rangle}{\partial t} + \langle \overline{u_j} \rangle \frac{\partial \langle \overline{u_i} \rangle}{\partial x_j} \right] = -\frac{\partial \langle \overline{p} \rangle}{\partial x_i} + \mu \frac{\partial^2 \langle \overline{u_i} \rangle}{\partial x_j^2} + \frac{\partial \langle \overline{\tau_{ij}} \rangle}{\partial x_j} - D_i$$

(2.2)

where ρ is fluid density, μ is molecular viscosity and $\tau_{ij} = -\rho \langle \overline{u_i' u_j'} \rangle - \rho \langle \overline{u_i}'' \overline{u_j}'' \rangle$ is macroscopic shear stress tensor, which consists of Reynolds stresses $(-\rho \langle \overline{u_i' u_j'} \rangle)$ due to temporal fluctuation and dispersive stresses $(-\rho \langle \overline{u_i}'' \overline{u_j}'' \rangle)$ due to spatial fluctuation.

The drag force D_i is resistance due to vegetation, the sum of form and viscous drag over the averaging scale.

$$D_i = \langle \frac{\partial \overline{p}''}{\partial x_i} \rangle - \langle \mu \frac{\partial^2 \overline{u_i}''}{\partial x_j^2} \rangle$$

(2.3)

Several approaches have been proposed for finite $R_e = \rho U d / \mu$ (d average diameter of grass), most of these proposed approaches use quadratic resistance law with $D_i = \rho C_N d N_g \langle \overline{u_i} \rangle |\langle \overline{u_i} \rangle|$, where N_g is average grass number density. Koch & Ladd (1997) have verified that a quadratic drag law describes the resistance due to array of cylinder from moderate to high Reynold numbers.

Since both dispersive stress $(-\rho \langle \overline{u_i}'' \overline{u_j}'' \rangle)$ and molecular stress $(\mu \; \partial u_i / \partial x_j)$ are

negligible compared to Reynolds stress $(-\rho\langle\overline{u_i' u_j'}\rangle)$, the equation 2.2 simplifies into

$$\frac{\partial\langle\overline{u_i}\rangle}{\partial x_i} = 0$$

$$\rho\left[\frac{\partial\langle\overline{u_i}\rangle}{\partial t} + \langle\overline{u_j}\rangle\frac{\partial\langle\overline{u_i}\rangle}{\partial x_j}\right] = -\frac{\partial\langle\overline{p}\rangle}{\partial x_i} - \rho\frac{\partial\langle\overline{u_i' u_j'}\rangle}{\partial x_j} - D_i$$

(2.4)

We further hypothesized that Reynolds stress can be estimated by using a constant eddy viscosity i.e.

$$-\rho\langle u_i' u_j'\rangle = \mu\left(\frac{\partial\overline{u_i}}{\partial x_j} + \frac{\partial\overline{u_j}}{\partial x_i}\right)$$

From now-onwards μ stands for eddy viscosity rather than molecular viscosity, with this simplification equation 2.2 further simplifies into

$$\frac{\partial\langle\overline{u_i}\rangle}{\partial x_i} = 0$$

$$\rho\left[\frac{\partial\langle\overline{u_i}\rangle}{\partial t} + \langle\overline{u_j}\rangle\frac{\partial\langle\overline{u_i}\rangle}{\partial x_j}\right] = -\frac{\partial\langle\overline{p}\rangle}{\partial x_i} + \mu\frac{\partial^2\langle\overline{u_i}\rangle}{\partial x_j^2} - \rho C_N d N_g\langle\overline{u_i}\rangle|\langle\overline{u_i}\rangle|$$

(2.5)

Boundary condition on the bed include no-shear, and a specified number density of grass. The no shear condition arises because, for dense vegetation the shear stress exerted by the bottom surface is expected to be negligible compared to the vegetation drag. On the surface, a rigid-lid condition (no shear and no normal velocity) or a free surface condition is suitable. In this analysis we have used rigid-lid condition on the top surface. The prediction of mean velocity made based on these condition agrees well with the experiments (e.g see Figure 3.1).

CHAPTER THREE

Linear stability analysis
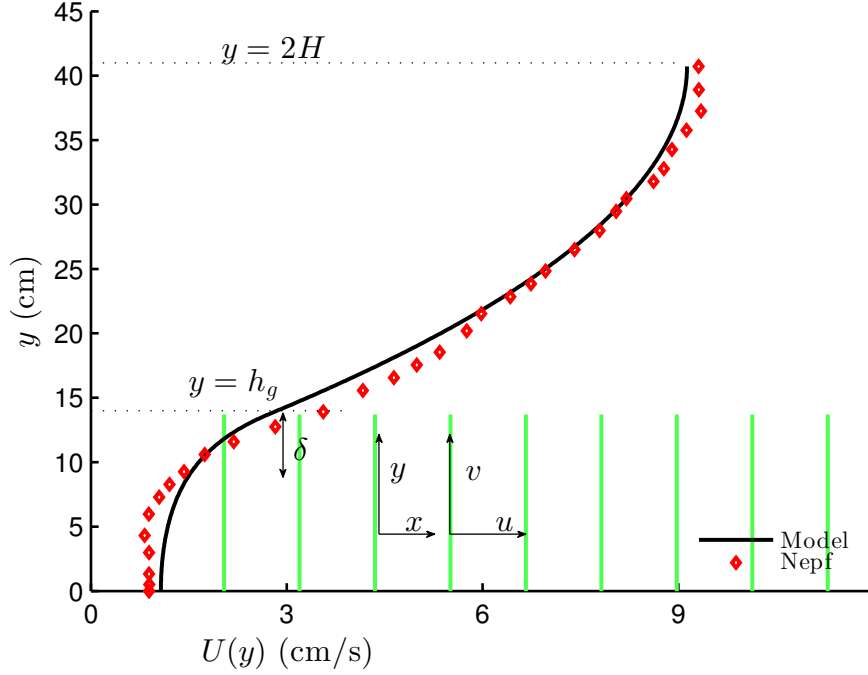
Figure 3.1: Schematic setup and comparison of our steady flow profile with that from the experiments in ref. [4] (Case I from Table 1) and its approximation with $U_0 = 7.28$ cm/s and $\delta = 5.02$ cm in our model. The grass extends up to $y = h_g$ in the water column of depth $2H$. The steady velocity profile can be decomposed into a parabolic profile in the unvegetated region, a uniform profile deep within the vegetation, and a boundary layer of thickness δ near the grass top. The dependence of the boundary layer thickness (estimated as $|U/U_y|$ at $y = h_g$ from the numerical solution of (3.1)) on the vegetation density parameter $R\tilde{N}_g$ is shown in the inset.

In order to understand nature of flow instability associated with monami, we first calculate the fully developed steady solution $\mathbf{u} = U(y)\hat{\boldsymbol{x}}$ of (2.5) driven by constant pressure gradient dP/dx, and use it to non-dimensionlize the mathematical model. The momentum balance (2.5) for $U(y)$ simplifies to

$$-\frac{dP}{dx} + \mu U''(y) - S(y)\rho C_N d N_g U |U| = 0, \tag{3.1}$$

where $S(y) = 1$ for $0 < y < h_g$ and $S(y) = 0$ for $h_g < y < 2H$. Eq. (3.1) is solved subject to no shear at the boundaries, i.e., $U'(0) = U'(2H) = 0$. The former arises for dense vegetation because the shear stress exerted by the bottom surface is expected to be negligible compared to the vegetation drag [?] whereas the latter models the free interface. A comparison of the steady flow profile from

the solution of (3.1) with experimental measurements is shown in Fig. The profile $U(y)$ has three distinct regions. Within the vegetation, it is approximately uniform with $U(y) \approx U_g = \sqrt{\frac{-dP/dx}{\rho C_N d N_g}}$, arising from a balance of the drag with the pressure gradient. Outside the vegetation, the velocity has a simple parabolic profile, similar to a Poissueille profile, influenced by the free shear at the surface. At the grass top, continuity of shear stresses results in a boundary layer of thickness δ - " one where shear does not arise from boundary conditions". Denoting U_{bl} to be the velocity scale in the boundary layer, and $U_0 = (-dP/dx)\, H^2/\mu$ the velocity scale in the unvegetated region, the balance between viscous forces and vegetation drag implies $(\mu U_{\mathrm{bl}}/\delta^2 \sim \rho C_N d N_g U_{\mathrm{bl}}^2)$, and the continuity of shear stress across the grass top implies $(U_{\mathrm{bl}}/\delta \sim U_0/H)$. Solving for δ and U_{bl} yields $\delta/H \sim U_{\mathrm{bl}}/U_0 \sim (R\tilde{N}_g)^{-1/3}$, A numerical estimate of δ (estimated as U/U_y at $y = h_g$) is compared with this prediction in Fig. 3.1 (inset). We identify the boundary layer to be analogous to the shear layer [8, 4] in the previous explanation of *monami*. This dependence of δ on N_g gives us a way to systematically investigate the effect of the shear layer thickness on the instability mechanism. Fig. 3.1 also shows that the asymptotic regime of a thin boundary layer is expected to hold for $R\tilde{N}_g \gtrsim 100$. In this notation, $U_g/U_0 = (R\tilde{N}_g)^{-1/2}$ (used later in deriving (4.3)).

Next we substitute $\mathbf{u} = (U + \tilde{u}, \tilde{v})$, $p = P + \tilde{p}$ in (??) and expand to linear order to investigate the evolution of small perturbations $(\tilde{u}, \tilde{v})$, which obey

$$\rho(u_t + U u_x + v U_y) = -p_x + \mu \nabla^2 u - 2S\rho C_N d N_g U u,$$

$$\rho(v_t + U v_x) = -p_y + \mu \nabla^2 v, \quad \nabla \cdot \mathbf{u} = 0,$$

where the tilde are dropped. These equations are non-dimensionalized using half channel height H, velocity U_0, and time H/U_0, leading to three non-dimensional parameters, *viz.* R, $\tilde{N}_g$, and the vegetation submergence ratio h_g/H. We also use

δ/H in lieu of $\tilde{N}_g$ to parametrize the vegetation density and help elucidate the instability mechanism. Using a stream function ψ with $u = \psi_y, v = -\psi_x$ to satisfy mass balance, we seek a solution of the form $(u, v, \psi) = (\hat{u}(y), \hat{v}(y), \phi(y)) \, e^{ikx+\sigma t}$ to obtain a modified Orr-Sommerfeld equation [3, 1, 2]

$$R^{-1} \left(D^2 - k^2\right)^2 \phi = \left[(\sigma + ikU)\left(D^2 - k^2\right) - ikU_{yy}\right]\phi + \tilde{N}_g D \left(2SUD\phi\right), \qquad (3.2)$$

where $D = d/dy$, and subject to the boundary conditions $\phi = D^2\phi = 0$ at $y = 0$ and $y = 2$. The growth rate σ for a given wave number k appears as an eigenvalue that allows a non-trivial solution ϕ of (3.2).

Chapter Four

Results

4.0.4 Unstable modes and critical parameters

In order to understand Critical criteria for waving we solve (3.2) numerically for σ and ϕ. A threshold in R, above which the flow is unstable $(\text{Re}(\sigma) > 0)$ for at least one k, emerges from the solution of (3.2). The dependence of this threshold R, and the corresponding marginally stable wavenumber k, on δ/H and h_g/H is shown in Fig. 4.1, and is found to compare well with experimental observations of [8]. The threshold R increases with the vegetation density, indicating a competition between the destabilizing shear in the flow, and the stabilizing effect of damping due to vegetation drag. The frequency $(\text{Im}(\sigma))$ of the fastest growing mode also agrees well with observed behavior – frequency of *monami*, maxima in the velocity spectra, and frequency of vortex passage in lab scale experiments [8] – for cases where the vegetation was sufficiently dense to be modeled by a continuum drag field as shown in Fig. 4.3. For completeness, the comparison of solution of (3.1) with the velocity profile observed in the lab scale experiment of [12] are shown in 4.4. The velocity profile for experiments of [8] are not available. The calculated velocity profiles for both these experiments are estimated using the constrain of given flow rate, grass number density and the submergence ratio. The experimentally observed *monami* wavelengths are not available for comparison. To better understand the instability mechanism, we consider the dependence of the fastest growing wavenumber on δ. The fastest growing wavenumber first increases proportional to H/δ, but at a critical δ discontinuously jumps and remains $O(1)$ (see Fig. 4.1). To aid in explaining this behavior, we show heat maps of $\text{Re}(\sigma)$ as a function of R and k, for different h_g/H and $\tilde{N}_g$ in Fig. 4.2. The smallest R on the neutral curve $(\text{Re}(\sigma) = 0)$ sets the threshold. We observe that as $\tilde{N}_g$ increases, the unstable region splits into two; we refer to the region with the higher k as "Mode 1", and the one with the lower k as "Mode 2". For $h_g/H \lesssim 0.9$, the unstable region for Mode 1 recedes to higher R, and
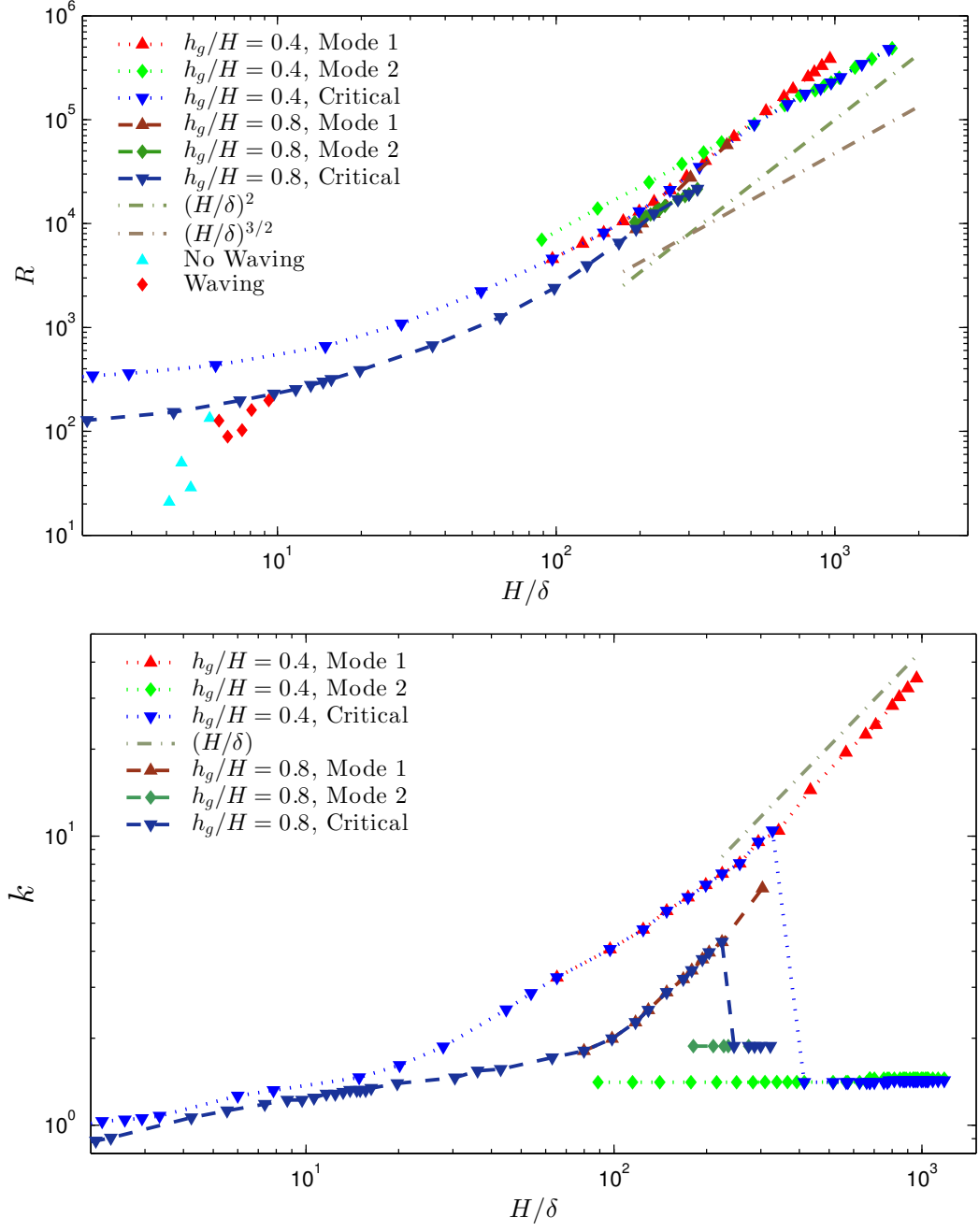
Figure 4.1: Critical Reynolds number, threshold Reynolds number for Mode 1 and Mode 2 (left) and the corresponding marginally stable wave number (right) for different submergence ratio as a function of vegetation density parametrized by the boundary layer thickness. Parameters from experiments reported by [8] to exhibit or suppress synchronous waving are also included in the left panel. In order to estimate the R for these experiments, a representative value of $\mu = 0.1$ Pa s was assumed.

Figure 4.2: Re(σ) and the neutral curve (Re(σ)=0) as a function of wavenumber and R for parameters shown in the corresponding panel. As $\tilde{N}_g$ increases, the unstable region splits into two labeled as "Mode 1" and "Mode 2". For $\tilde{N}_g$ below (above) a critical value, Mode 1 (Mode 2) sets the threshold R.

for $h_g/H \gtrsim 0.9$, the region shrinks to zero size. In either case, due to such behavior the most unstable mode transitions discontinuously from Mode 1 to Mode 2. All experime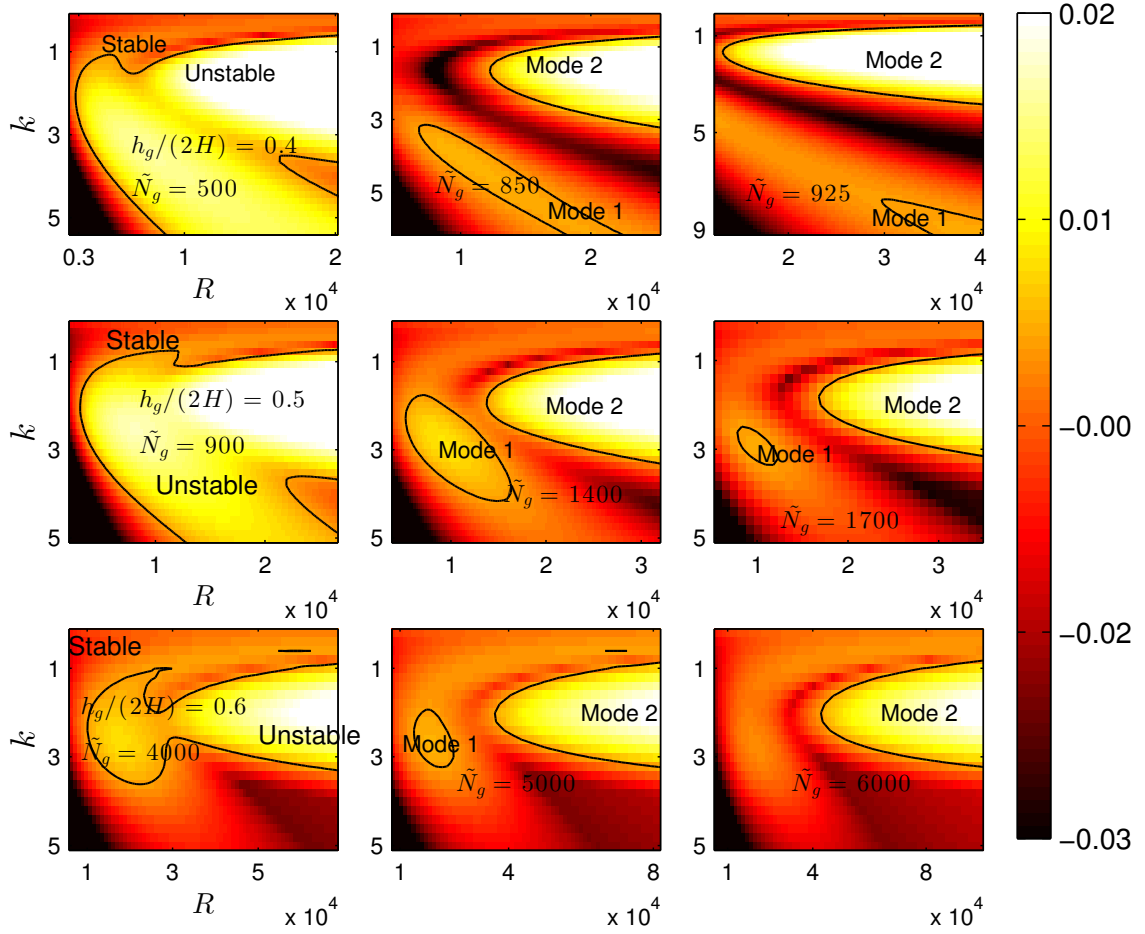ntal data we have found corresponds to a vegetation density for which the unstable region in the $R - k$ space has not split into two. The distinct asymptotic behavior of the two modes as $\tilde{N}_g \gg 1$ distinguish them from each other and facilitate comparison with KH instability mechanism.

4.0.5 Mode 1

We numerically observe that the threshold Reynolds number for Mode 1 instability scales as $R \sim (H/\delta)^2$ (or $R \propto \tilde{N}_g^2$). Our calculations also show that Mode 1 asymptotically localizes to the boundary layer near the grass top, and exhibits highest growth for a perturbation of $k \sim H/\delta$ (see Fig. 4.1). The behavior of this critical Reynolds number can be understood by considering the limit $R \gg 1$ and $\tilde{N}_g \gg 1$. Estimating the size of various terms of (3.2) within the boundary layer in this limit help us understand the behavior of the critical R. Using $D \sim H/\delta$, $\sigma \sim O(1)$, and $U = U_{\text{bl}} \sim \delta/H$ in the boundary layer; the magnitude of the advection term is $(H/\delta)^2$ (or $R^{2/3}\tilde{N}_g^{2/3}$), and the viscous and vegetation drag terms are $(1/R)(\delta/H)^{-4}$ (or $(R^{1/3}\tilde{N}_g)^{4/3}$). The advection term, viscous term and vegetation drag terms balance when $R \sim (H/\delta)^2$ (or $R \sim \tilde{N}_g^2$).

To further understand the mechanism of Mode 1, we rescale (3.2) near the grass-top using the the boundary layer scalings $\eta = y/(\delta/H)$, $U(y) = (\delta/H)\overline{U}(\eta)$ and $k = (H/\delta)\overline{k}$. With these scalings (3.2) simplifies to

$$\left(\overline{D}^2 - \overline{k}^2\right)^2 \phi = (R/\tilde{N}_g^2)^{1/3}\left[(\sigma + i\overline{kU})\left(\overline{D}^2 - \overline{k}^2\right) - i\overline{kU}_{\eta\eta}\right]\phi + \overline{D}\left(2S\overline{UD}\phi\right),$$

$$(4.1)$$
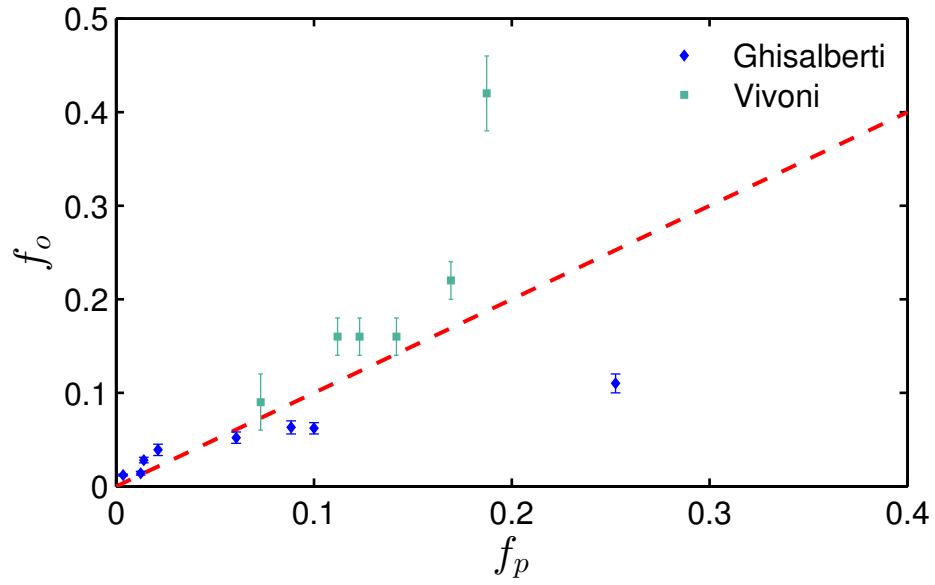
Figure 4.3: Comparison of experimental observations of the experimentally measured dominant frequency f_o (in Hz) with the predictions $f_p = \text{Im}(\sigma)$ from the solution of (3.2). The experimental data in the inset is obtained from [8] (Ghisalberti) and [12] (Vivoni). In order to estimate the R for these experiments, a representative value of $\mu = 0.1$ Pa s was assumed.
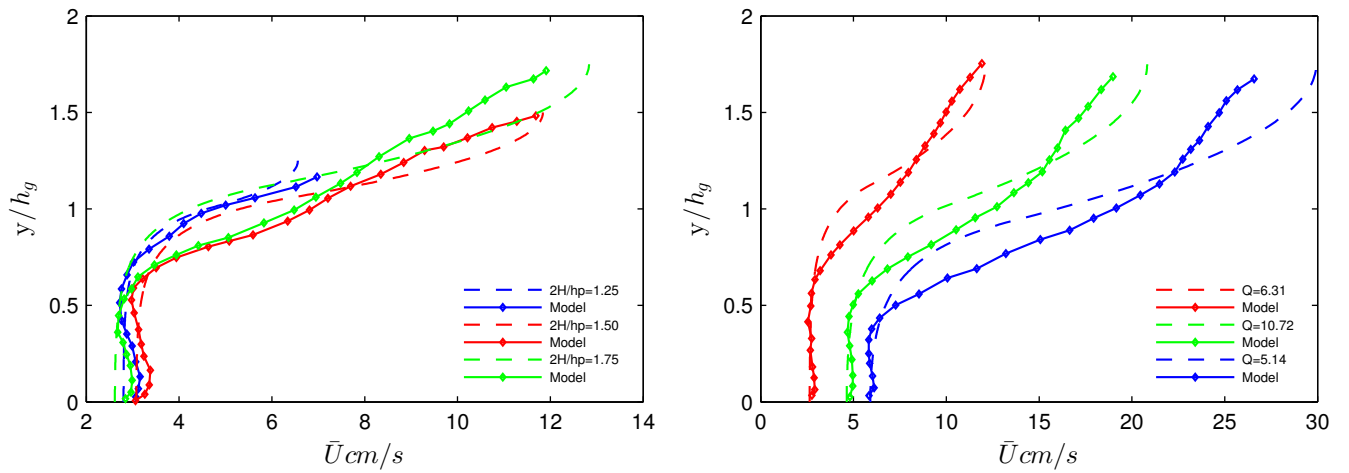
Figure 4.4: Comparison of experimental velocity profile of lab scale experiments with the solution of (3.1) for *Case A* and *Case B* experimental observation of [12]

in a region of thickness $O(\delta)$ near $y = h_g$, where $\overline{D} = d/d\eta$. Since $(R/\tilde{N}_g^2)$ is the only remaining parameter in (4.1), the mode shape and solution are expected to converge in the limit $R \gg 1$, $\tilde{N}_g \gg 1$, but $R/\tilde{N}_g^2$ fixed. Our numerical findings confirm this expectation; the critical R scales as $(H/\delta)^2$ as shown in Fig. 4.1 and the mode shapes are self-similar with length scale δ, as shown in Fig 4.5.

Mode 1 shares many characteristics with the KH instability (see Table 4.1). The fastest growing wavenumber at the critical R scales as $k \propto (H/\delta)$, similar to KH instability. The extent of the unstable mode is also localized to the boundary layer region. The porous nature of the vegetation implies that a weak flow of magnitude $U_{\rm bl} = U_0 \delta/H$ penetrates a thin boundary layer region δ, and therefore the shear gradient $U_{yy} \sim U_0/\delta H$ is largest in this region. The strong shear gradient U_{yy} in the boundary layer plays a central role in destabilizing the flow and localizing the instability to that region. Our detailed description of Mode 1, given by (4.1) also highlights key differences with formulations of KH. KH is usually described using the inviscid Rayleigh's equation,

$$(\sigma + ikU)\left(D^2 - k^2\right)\phi = ikU_{yy}\phi, \qquad (4.2)$$

and is therefore not parametrized by the Reynolds number. Describing the instability using the Orr-Sommerfeld equation introduces the Reynolds number as a parameter, but shear flows with tanh-profiles are unstable for all values of the parameter Drazin81. Therefore, based on the inviscid formulations of KH instability, the origin of the threshold flow conditions observed in experiments and the field is unclear.

In our model, (turbulent eddy) viscosity sets the scale of the boundary layer, and therefore for Mode 1. However, the boundary layer is established only in the vegetated region; the velocity profile does not saturate on the scale of δ in the
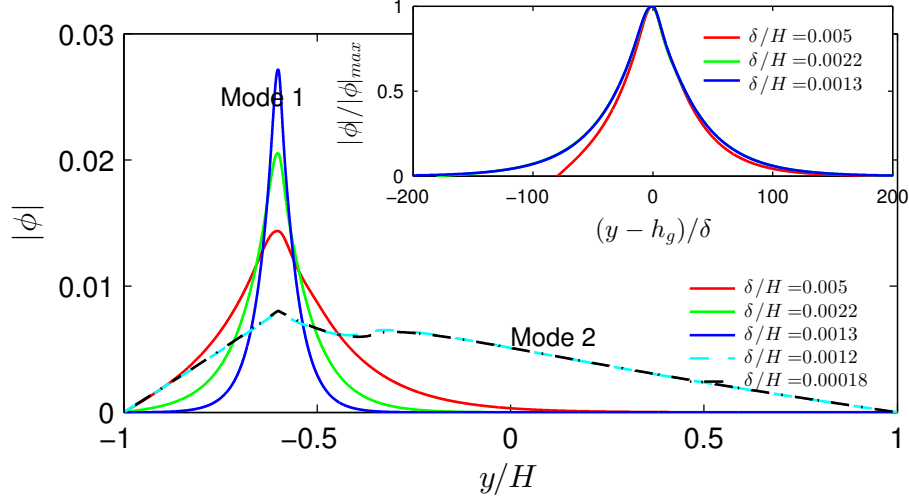
Figure 4.5: Plot of the neutral Mode 1 (solid) and Mode 2 (dashed) shape $|\phi|$ in the limit of small δ/H for $h_g/H = 0.2$. The approach of mode shapes to each other for these small values of δ/H indicates that the dense vegetation asymptote is reached. Mode 1 shapes appear self-similar in shape as $\delta \to 0$. Inset shows rescaled $|\phi|$ for Mode 1 as a function of $(y - h_g)/\delta$ approach a universal shape, indicating that an asymptotic limit has been reached.

unvegetated region. The threshold flow condition arises from a competition between the destabilizing role of fluid inertia, which is very similar to the one played in KH, and the vegetation drag. The vegetation drag may not be neglected within this boundary layer, and therefore plays a central role in the Mode 1 instability mechanism.

4.0.6 Mode 2

The threshold condition for Mode 2 is numerically observed to be $R \propto (\delta/H)^{-3/2}$ (or $R \propto \tilde{N}_g$) for $k \sim O(1)$, shown in Fig. 4.1, which can be understood by assuming $R \gg 1$ but fixed $R/\tilde{N}_g \sim O(1)$. In this limit, the non-dimensional flow in the grass bed is $U_g/U_0 \sim (R\tilde{N}_g)^{-1/2} \ll 1$, and therefore $ikU \ll \sigma$ may be neglected in comparison to σ. Furthermore, U_{yy} decays to zero within the grass outside the boundary layer . Outside the grass, the turbulent viscous stress term is negligible

compared to the inertial term because $R \gg 1$. Thus, (3.2) simplifies to

$$\sigma \left(D^2 - k^2 \right) \phi = -2(\tilde{N}_g/R)^{1/2} D^2 \phi, \quad \text{for } y < h_g \tag{4.3a}$$

$$(\sigma + ikU) \left(D^2 - k^2 \right) \phi = ikU_{yy}\phi, \quad \text{for } y > h_g. \tag{4.3b}$$

The only remaining parameter in (4.3) is $R/\tilde{N}_g$. For fixed $R/\tilde{N}_g$, the mode shape converges in the aforementioned limit, in agreement with our numerical results shown in Fig. 4.5. This convergence indicates that we have identified the correct asymptotic limit to investigate Mode 2. The parameter $R/\tilde{N}_g$ therefore sets the threshold, justifying the numerically observed asymptotic behavior $R \propto \tilde{N}_g$ (or $R \sim (\delta/H)^{-3/2}$; see Fig. 4.1 for comparison with numerical results). The structure of this mode in the aforementioned limit is such that ϕ is continuous at $y = h_g$, but $D\phi$ undergoes a rapid transition there, on the scale of boundary layer thickness δ. The eigenvalues and the mode shape are otherwise independent of δ. Therefore we conclude that the boundary layer only plays a secondary role of regularizing the discontinuity in tangential velocity arising at $y = h_g$ in this instability mechanism. The enhanced shear in the boundary layer plays no role for this mode of instability. Mode 2 has characteristics distinct from KH. Outside the grass, the unstable mode shape is governed by the inviscid Rayleigh's equation (4.2). An inflection point in $U(y)$ is a necessary condition for instability arising from (4.2) according to Rayleigh's criteria Rayleigh1879. However, for our $U(y)$ profiles, $U_{yy}(y) = -1$ above the grass and therefore does not change sign for $y > h_g$. Instead, the dynamics are coupled with the flow in the grass bed described by (4.3a) in $y < h_g$. The absence of U_{yy} in (4.3a) indicates that U_{yy} is approximated to be zero in $y < h_g$, and therefore the positive values of U_{yy} that occurs in the boundary layer do not affect this mode of instability to leading order. Furthermore, the presence of the critical parameter $R/\tilde{N}_g$ in (4.3a) indicates the presence of alternative destabilizing dynamics, involving the interaction

	KH	Mode 1	Mode 2
Base velocity profile	$U(y) = U_0 \tanh(y/\delta)$	Equation (3.1)	
Domain	$-\infty < y < \infty$	$-1 < y < 1$	
Inflection point	exists at $y = 0$	$U''(y)$ discontinuous at $y = h_g$	
Shear layer thickness	δ	$\delta \sim H \left(R \tilde{N}_g \right)^{-1/3}$	
Linearized dynamics	Equation (4.2)	Equation (3.2)	
Dense grass limit	no grass included	Equation (4.1)	Equation (4.3)
Critical parameters	none	$R \propto \tilde{N}_g^2$	$R \propto \tilde{N}_g$
Most unstable k as $\delta \to 0$	$\propto H/\delta$	$\propto H/\delta$	$O(1)$
Mode localized?	yes, near $y = 0$	yes, near $y = h_g$	no, spans water column

Table 4.1: Comparison between KH instability and the two unstable modes resulting from solution of 3.2.

of flow in the unvegetated region governed by (4.2) with the flow in the vegetated region incorporating the drag. Therefore, we conclude that Mode 2 is distinct from the KH instability, and owes its existence to vegetation drag.

CHAPTER FIVE

Discussion

5.0.7 Role of turbulence Model

We have modeled turbulence using a constant eddy viscosity. The simplicity of this model allows us to make progress and capture the essential features of the instability. However, this simplicity in some cases only provides a qualitatively accurate description of the flow. In this subsection, we present an account of the advantages and shortcomings of assuming a constant eddy viscosity to model the turbulence.

As a consequence of the constant eddy viscosity, the boundary layer thickness δ scales as $H(R\tilde{N}_g)^{-1/3}$. Experimental observations show that the boundary layer thickness scales instead as $\tilde{N}_g^{-1}$ [10]. Whereas the precise boundary layer thickness is governed by the details of the turbulence model, the existence of this boundary layer for dense vegetation is independent of the turbulence model. We have captured one possible realization of this feature using constant eddy viscosity. Experiments have also shown that a model based on mixing length l better approximates the turbulent characteristics of the flow with $l \sim \delta$; *i.e.*, the boundary layer itself establishes eddies to transport momentum. The eddy viscosity corresponding to this model is $\mu \sim \rho U \delta$, and the leading order balance between turbulent momentum transport and vegetation drag is $\mu U/\delta^2 \sim \rho C_N d N_g U^2$. Substituting μ yields $\delta/H \sim \tilde{N}_g^{-1}$, in agreement with the experimental observations.

Within our framework, the mixing length model implies a scale for the eddy viscosity $\mu \sim \rho U_{\text{bl}} \delta$ at grass top, which corresponds to an effective $R \sim U_0 H/U_{\text{bl}} \delta$. Furthermore, matching the slope of the velocity profile from the boundary layer to the unvegetated flow implies $U_{\text{bl}}/U_0 \sim \delta/H$, and therefore $R \sim (H/\delta)^2$. Substituting this relation in $\delta/H \sim (R\tilde{N}_g)^{-1/3}$ and solving for δ yields $\delta/H \sim \tilde{N}_g^{-1}$. This simple scaling analysis shows that the boundary layer thickness depends on the turbulence model, and indicates that turbulence models based on mixing lengths will yield more

realistic scalings for boundary layer thickness. At the same time, the qualitative features of the instability are represented by our analysis.

The Mode 1 instability is driven by the intense shear on the scale of the boundary layer. The driving mechanism for this instability is similar to that of KH, and relies only on the presence of this shear as presented in the $\overline{U}_{\eta\eta}$ term in equation (4.1). Therefore, we expect Mode 1 instability to be exhibited independent of the turbulence model. We further expect the fastest growing wavenumber to be proportional to $1/\delta$, and the mode to be localized to the boundary layer because these results have a basis in dimensional analysis. The threshold parameters for Mode 1, however, may depend on the precise turbulence model used.

For the Mode 2 instability, the turbulent momentum transport is found to be irrelevant to leading order. In the asymptotic limit of dense grass, (4.3) shows that the instability is driven by the interaction of the unvegetated flow with the vegetation drag. The influence of the turbulence model is limited to the regularization of the sharp transition in tangential velocity across the grass top. Therefore we expect Mode 2 and its features to be preserved even if a different turbulence model is used.

5.0.8 Comparison with previous models

A modified version of the Orr-Sommerfeld equation was analyzed previously by [2], [1], and [13] in the context of instabilities in depth-averaged shallow water flows, where bottom friction replaces or augments vegetation drag. They assumed the steady profile to be a hyperbolic tangent, the drag to be isotropic, and the flow domain to be infinite in y. White07 also neglected the eddy viscosity in their stability analysis. While a detailed investigation needed to compare the consequence of

the different assumptions is outside the scope of this paper, we discuss similarities and differences between their results and ours. These investigations only found one unstable mode. It is most likely so because the calculations were restricted to a parameter regime where the two modes have not yet been separated from each other, as is the case shown in Fig. 4.2 for the lowest $\tilde{N}_g$. These investigations also found that increasing the drag could further destabilize the flow, which is consistent with our interpretation of the Mode 2 instability mechanism.

The analogous oscillation of terrestrial canopies in wind, known as *Honami* [7, 11], is different because the atmospheric boundary layer is much larger than the vegetation height. In the framework of our model, the limit of $h_g/H \ll 1$ while δ/h_g = constant can be used to represent the hydrodynamic instability for the terrestrial case. We find that in this case, the transition from Mode 1 to Mode 2 happens at such a large vegetation density, that Mode 2 is irrelevant. Hence, only the KH-like characteristics are observed in the terrestrial case.

CHAPTER SIX

Conclusion

Appendix A

Stuff Too Complicated To Talk About

Appendix B

Stuff Too Boring to Talk About

Bibliography

[1] D. Chen and G. H. Jirka. Absolute and convective instabilities of plane turbulent wakes in a shallow water layer. *Journal of Fluid Mechanics*, 338:157–172, 1997.

[2] V. H. Chu, J-H Wu, and R. E. Khayat. Stability of transverse shear flows in shallow open channels. *Journal of Hydraulic Engineering*, 117(10):1370–1388, 1991.

[3] P. G. Drazin and W. H. Reid. Hydrodynamic stability. *Cambridge U. Press, Cambridge*, 1981.

[4] M. Ghisalberti and H. M. Nepf. The limited growth of vegetated shear layers. *Water Resources Research*, 40(7), 2004.

[5] M. Ghisalberti and H. M. Nepf. The sructures of shear layer in flows over rigid and flexible canopies. *Enviornmental Fluid Mechanics*, pages 277–301, 2006.

[6] R. E. Grizzle, F. T. Short, C. R. Newell, H. Hoven, and L. Kindblom. Hydrodynamically induced synchronous waving of seagrasses: 'monami' and its possible effects on larval mussel settlement. *Journal of Experimental Marine Biology and Ecology*, 206(1–2):165–177, 1996.

[7] E. Inoue. Studies of the Phenomena of Waving Plants Caused by Wind. *J. of Agri. Meteor.*, 11(4):147–151, 1956.

[8] M. Ghisalberti and H. M. Nepf. Mixing layer and cohrent structures in vegetated aquatic flows. *J. Geophys. Res.*, 107, 2002.

[9] H. M. Nepf and E. R. Vivoni. Flow structure in depth-limited vegetated flow. *J. Geophys. Res.*, 105:28,547–28,557, 2000.

[10] H. M. Nepf, B. White, and E. Murphy. Retention time and dispersion associated with submerged aquatic canopies. *Water Resources Research*, 43, 2007.

[11] M. R. Raupach, J. J. Finnigan, and Y.Brunet. Cohrent eddies and turbulence in vegetation canopies: The mixing layer analogy. *Boundary-Layer Meteorology*, 78:351–382, 1996.

[12] E. R. Vivoni. Turbulence structure of a model seagrass meadow. Master's thesis, MIT, 1998.

[13] B. L. White and H. M. Nepf. Shear instability and coherent structures in shallow flow adjacent to a porous layer. *Journal of Fluid Mechanics*, 593:1–32, 2007.